Stanford Exploration Project, Report 114, October 14, 2003, pages 1–??

Seismic attenuation due to wave-induced flow

Steven R. Pride, James G. Berryman, and Jerry M. Harris[1]

ABSTRACT

Analytical expressions for three P-wave attenuation mechanisms in sedimentary rocks are given a unified theoretical framework. Two of the models concern wave-induced flow due to heterogeneity in the elastic moduli at "mesoscopic" scales (scales greater than grain sizes but smaller than wavelengths). In the first model, the heterogeneity is due to lithological variations (*e.g.*, mixtures of sands and shales) with a single fluid saturating all the pores. In the second model, a single uniform lithology is saturated in mesoscopic "patches" by two immiscible fluids (e.g., air and water). In the third model, the heterogeneity is at "microscopic" grain scales (broken grain contacts and/or micro-cracks in the grains) and the associated fluid response corresponds to "squirt flow." The model of squirt flow derived here reduces to proper limits as any of the fluid bulk modulus, crack porosity, and/or frequency is reduced to zero. It is shown that squirt flow is incapable of explaining the measured level of loss ($10^{-2} < Q^{-1} < 10^{-1}$) within the seismic band of frequencies (1 to 10^4 Hz); however, either of the two mesoscopic scale models easily produce enough attenuation to explain the field data.

INTRODUCTION

Intrinsic seismic attenuation is often quantified by the inverse quality factor Q^{-1} of sedimentary rock within the seismic band of frequencies, which we loosely define as 1 to 10^4 Hz. For transmission experiments (earthquake recordings, VSP, cross-well tomography, sonic logs), the total measured attenuation can be decomposed as $Q^{-1}_{\rm total} = Q^{-1}_{\rm scat} + Q^{-1}$ where both contributions to the total attenuation are necessarily positive. The inverse quality factor Q^{-1} for the intrinsic attenuation represents the fraction of wave energy irreversibly lost to heat during a wave period as normalized by the strain energy. For refletion seismic prospecting, there are other wave energy losses due to reflection and transmission effects at interfaces. These effects are neglected here for reflection seismic by exclusion. For the types of transmission experiments that we do consider here, we justify neglecting them since we are basically studying the losses within any single block of material, and not treating effects at interfaces between blocks since these can be handled independently with well-known methods.

Crosswell experiments in horizontally-stratified sediments produce negligible amounts of scattering loss so that essentially all loss is attributable to intrinsic attenuation. Quan and Harris (1997) use tomography to invert for the amplitudes of crosswell P-wave first arrivals

[1]**email:** SRPride@lbl.gov,berryman@pangea.stanford.edu,harris@pangea.stanford.edu

to obtain the Q^{-1} for the layers of a stratified sequence of shaly sandstones and limestones (depths ranging from 500–900 m). The center frequency of their measurements is roughly 1750 Hz and they find that $10^{-2} < Q^{-1} < 10^{-1}$ for all the layers in the sequence. Sams *et al.* (1997) also measure the intrinsic loss in a stratified sequence of water-saturated sandstones, siltstones and limestones (depths ranging from 50–250 m) using VSP (30–280 Hz), crosswell (200–2300 Hz), sonic logs (8–24 kHz), and ultrasonic laboratory (500–900 kHz) measurements. Sams *et al.* (1997) calculate (with some inevitable uncertainty) that in the VSP experiments, $Q^{-1}/Q_{\rm scat}^{-1} \approx 4$, while in the sonic experiments, $Q^{-1}/Q_{\rm scat}^{-1} \approx 19$; i.e., for this sequence of sediments, the intrinsic loss dominates the scattering loss at all frequencies. Sams *et al.* (1997) also find $10^{-2} < Q^{-1} < 10^{-1}$ across the seismic band.

We demonstrate here that wave-induced fluid flow generates enough heat to explain these measured levels of intrinsic attenuation. Other attenuation mechanisms need not be considered, although they may in fact be present but contribute much smaller fractions of the overall observed attenuation. The induced flow occurs at many different spatial scales that can broadly be categorized as "macroscopic", "mesoscopic", and "microscopic."

The macroscopic flow is the wavelength-scale equilibration occuring between the peaks and troughs of a P-wave. This mechanism was first treated by Biot (1956a) and is often simply called "Biot loss." However, the flow at such macro scales drastically underestimates the measured loss in the seismic band (by as much as 5 orders of magnitude). Mavko and Nur (1979) therefore proposed a microscopic mechanism due to microcracks in the grains and/or broken grain contacts. When a seismic wave squeezes a rock having such grain-scale damage, the cracks respond with a greater fluid pressure than the main porespace resulting in a flow from crack to pore that Mavko and Nur (1979) named "squirt flow." Dvorkin *et al.* (1995) have given a squirt-flow model applicable to liquid-saturated rocks. Although squirt flow seems entirely capable of explaining much of the measured attenuation in the laboratory at ultrasonic frequencies and may also turn out to be important for propagation in ocean sediments at ultrasonic frequencies (Williams et al., 2002) as well, we show here that this mechanism cannot explain the attenuation in the seismic band.

Thus, a third mechanism based on mesoscopic-scale heterogeneity seems required to explain seismic attenuation. Mesoscopic length scales are those larger than grain sizes but smaller than wavelengths. Heterogeneity across these scales may be due to lithological variations or to patches of different immiscible fluids. When a compressional wave squeezes a material containing mesoscopic heterogeneity, the effect is similar to squirt with the more compliant portions of the material responding with a greater fluid pressure than the stiffer portions. There is a subsequent flow of fluid capable of generating significant amounts of loss in the seismic band.

Prior models of such mesoscopic loss have focused on flow between the layers of a stratified material due to P-waves propagating normal to the layering [e.g., White *et al.* (1975), Norris (1993), Gurevich and Lopatnikov (1995), and Gelinksy and Shapiro (1997)]. The present study seeks to model the flow for arbitrary mesoscopic geometry, albeit under the restriction that only two porous phases are mixed together in each averaging volume.

In the next section, we review a recent model of Pride and Berryman (2003a,b) treating

the mesoscopic loss created by lithological patches having, for example, different degrees of consolidation. This so-called "double-porosity" model provides the theoretical framework that will be used throughout. Then, we derive a new patchy-saturation variant of the model and, in following section, a new squirt-flow variant. The results are then discussed in the concluding section. The main point of the paper is to derive models for patchy-saturation and squirt using the same notation and approach as the double-porosity theory; in so doing, we aim to draw conclusions about the nature of attenuation in the seismic band of frequencies.

REVIEW OF THE DOUBLE-POROSITY THEORY

In this theory, the mesoscopic heterogeneity is modeled as being a mixture of two porous phases saturated by a single fluid. Porous phase 1 is defined as being the stiffer lower-permeability phase and phase 2 the more compressible higher-permeability phase.

Local Governing Equations

Each porous phase is locally modeled as a porous continuum and obeys the laws of poroelasticty [*e.g.*, Biot (1962)]

$$\nabla \cdot \boldsymbol{\tau}_i^D - \nabla p_{ci} = \rho \ddot{\mathbf{u}}_i + \rho_f \dot{\mathbf{Q}}_i \tag{1}$$

$$\mathbf{Q}_i = -\frac{k_i}{\eta}\left(\nabla p_{fi} + \rho_f \ddot{\mathbf{u}}_i\right) \tag{2}$$

$$\begin{bmatrix} \nabla \cdot \dot{\mathbf{u}}_i \\ \nabla \cdot \mathbf{Q}_i \end{bmatrix} = -\frac{1}{K_i^d}\begin{bmatrix} 1 & -\alpha_i \\ -\alpha_i & \alpha_i/B_i \end{bmatrix}\begin{bmatrix} \dot{p}_{ci} \\ \dot{p}_{fi} \end{bmatrix} \tag{3}$$

$$\boldsymbol{\tau}_i^D = G_i\left(\nabla \mathbf{u}_i + \nabla \mathbf{u}_i^T - \frac{2}{3}\nabla \cdot \mathbf{u}_i \mathbf{I}\right) \tag{4}$$

where the index i represents the two phases ($i = 1, 2$). The response fields in these equations are themselves local volume averages taken over a scale larger than the grain sizes but smaller than the mesoscopic extent of either phase. The local fields are: $\mathbf{u}_i$, the average displacement of the framework of grains; $\mathbf{Q}_i$, the Darcy filtration velocity; p_{fi}, the fluid pressure; p_{ci}, the confining pressure (total average pressure); and $\boldsymbol{\tau}_i^D$, the deviatoric (or shear) stress tensor. In the linear theory of interest here, the overdots on these fields denote a partial time derivative. In the local Darcy law (2), η is the fluid viscosity and the permeability k_i is a linear time-convolution operator whose Fourier transform $k_i(\omega)$ is called the "dynamic permeability" and can be modeled using the theory of Johnson *et al.* (1987) (see the Appendix).

In the local compressibility law (3), K_i^d is the drained bulk modulus of phase i (confining pressure change divided by sample dilatation under conditions where the fluid pressure does not change), B_i is Skempton's (1954) coefficient of phase i (fluid pressure change divided by confining pressure change for a sealed sample), and α_i is the Biot and Willis (1957) coefficient of phase i defined as

$$\alpha_i = (1 - K_i^d/K_i^u)/B_i, \tag{5}$$

where K_i^u is the undrained bulk modulus (confining pressure change divided by sample dilatation for a sealed sample). In the present work, no restrictions to single-mineral isotropic grains will be made. Finally, in the deviatoric constitutive law (4), G_i is the shear modulus of the framework of grains. At the local level, all these poroelastic constants are taken to be real constants. In the appendix we give the Gassmann (1951) fluid-substitution relations that allow B_i and α_i to be expressed in terms of the porosity ϕ_i, the fluid and solid bulk moduli K_f and K_s, and the drained modulus K_i^d.

Double-Porosity Governing Equations

In the double-porosity model, the goal is to determine the average fluid response in each of the porous phases in addition to the average displacement of the solid grains (Berryman and Wang, 1995; 2000). The averages are taken over regions large enough to significantly represent both porous phases, but smaller than wavelengths. Assuming an $e^{-i\omega t}$ time dependence, Pride and Berryman (2003a) have found the volume averaged local laws (1)–(4) in order to obtain the macroscopic "double-porosity" governing equations in the form

$$\nabla\cdot\boldsymbol{\tau}^D - \nabla P_c = -i\omega(\rho\mathbf{v}+\rho_f\mathbf{q}_1+\rho_f\mathbf{q}_2), \tag{6}$$

$$\begin{bmatrix}\mathbf{q}_1\\ \mathbf{q}_2\end{bmatrix} = -\frac{1}{\eta}\begin{bmatrix}\kappa_{11} & \kappa_{12}\\ \kappa_{12} & \kappa_{22}\end{bmatrix}\cdot\begin{bmatrix}\nabla\overline{p}_{f1}-i\omega\rho_f\mathbf{v}\\ \nabla\overline{p}_{f2}-i\omega\rho_f\mathbf{v}\end{bmatrix}, \tag{7}$$

$$\begin{bmatrix}\nabla\cdot\mathbf{v}\\ \nabla\cdot\mathbf{q}_1\\ \nabla\cdot\mathbf{q}_2\end{bmatrix} = i\omega\begin{bmatrix}a_{11} & a_{12} & a_{13}\\ a_{12} & a_{22} & a_{23}\\ a_{13} & a_{23} & a_{33}\end{bmatrix}\cdot\begin{bmatrix}P_c\\ \overline{p}_{f1}\\ \overline{p}_{f2}\end{bmatrix}+i\omega\begin{bmatrix}0\\ \zeta_{\rm int}\\ -\zeta_{\rm int}\end{bmatrix}, \tag{8}$$

$$-i\omega\zeta_{\rm int} = \gamma(\omega)(\overline{p}_{f1}-\overline{p}_{f2}), \tag{9}$$

$$-i\omega\boldsymbol{\tau}^D = [G(\omega)-i\omega g(\omega)]\left[\nabla\mathbf{v}+(\nabla\mathbf{v})^T-\frac{2}{3}\nabla\cdot\mathbf{v}\mathbf{I}\right]. \tag{10}$$

The macroscopic fields are: $\mathbf{v}$, the average particle velocity of the solid grains throughout an averaging volume of the composite; $\mathbf{q}_i$, the average Darcy flux across phase i; P_c, the average total pressure in the averaging volume; $\boldsymbol{\tau}^D$, the average deviatoric stress tensor; $\overline{p}_{fi}$, the average fluid pressure within phase i; and $-i\omega\zeta_{\rm int}$, the average rate at which fluid volume is being transferred from phase 1 into phase 2 as normalized by the total volume of the averaging region. The dimensionless increment $\zeta_{\rm int}$ represents the "mesoscopic flow."

Equation (7) is the generalized Darcy law allowing for fluid cross-coupling between the phases [*c.f.*, Pride and Berryman (2003b)], equation (8) is the generalized compressibility law where $\nabla\cdot\mathbf{q}_i$ corresponds to fluid that has been depleted from phase i due to transfer across the external surface of an averaging volume, and equation (9) is the transport law for internal mesoscopic flow (fluid transfer between the two porous phases).

The coefficients in these equations have been modeled by Pride and Berryman (2003a,b). Before presenting these results, the nature of the waves implicitly contained in these laws is briefly commented upon. If plane-wave solutions for $\mathbf{v}$, $\mathbf{q}_1$ and $\mathbf{q}_2$ are introduced, there is found to be a single transverse wave, and three longtitudinal responses: a fast wave and

two slow waves (Berryman and Wang, 2000). The fast wave is the usual P-wave identified on seismograms, while the two slow waves correspond to fluid-pressure diffusion in phases 1 and 2. The only problem with analyzing the fast compressional wave in this manner is that the characteristic equation for the longtitudinal slowness s is cubic in s^2 and, therefore, analytically inconvenient.

Reduction to an Effective Biot Theory

The approach that we take instead is to first reduce these double-porosity laws (6)–(10) to an effective single-porosity Biot theory having complex frequency-dependent coefficients. The easiest way to do this is to assume that phase 2 is entirely embedded in phase 1 so that the average flux $\mathbf{q}_2$ into and out of the averaging volume across the external surface of phase 2 is zero. By placing $\nabla \cdot \mathbf{q}_2 = 0$ into the compressibility laws (8), the fluid pressure p_{f2} can be entirely eliminated from the theory. In this case the double-porosity laws reduce to effective single-porosity poroelasticity governed by laws of the form (3) but with effective poroelastic moduli given by

$$\frac{1}{K_D} = a_{11} - \frac{a_{13}^2}{a_{33} - \gamma/i\omega}, \tag{11}$$

$$B = \frac{-a_{12}(a_{33} - \gamma/i\omega) + a_{13}(a_{23} + \gamma/i\omega)}{(a_{22} - \gamma/i\omega)(a_{33} - \gamma/i\omega) - (a_{23} + \gamma/i\omega)^2}, \tag{12}$$

$$\frac{1}{K_U} = \frac{1}{K_D} + B\left(a_{12} - \frac{a_{13}(a_{23} + \gamma/i\omega)}{a_{33} - \gamma/i\omega}\right). \tag{13}$$

Here, $K_D(\omega)$ is the effective drained bulk modulus of the double-porosity composite, $B(\omega)$ is the effective Skempton's coefficient, and $K_U(\omega)$ is the effective undrained bulk modulus. An effective Biot-Willis constant can then be defined using $\alpha(\omega) = [1 - K_D(\omega)/K_U(\omega)]/B(\omega)$.

The complex frequency dependent "drained" modulus K_D again defines the total volumetric response when the average fluid pressure throughout the entire composite is unchanged; however, the local fluid pressure in each phase may be non-uniform even though the average is zero resulting in mesoscopic flow and in K_D being complex and frequency dependent. Similar interpretations hold for the undrained moduli K_U and B. An undrained response is when no fluid can escape or enter through the external surface of an averaging volume; however, there can be considerable internal exchange of fluid between the two phases resulting in the complex frequency-dependent nature of both K_U and B.

Double-Porosity a_{ij} Coefficients

The constants a_{ij} are all real and correspond to the high-frequency response for which no internal fluid-pressure relaxation can take place. They are given exactly as (Pride and Berryman, 2003a)

$$a_{11} = 1/K \tag{14}$$

$$a_{22} = \frac{v_1\alpha_1}{K_1^d}\left(\frac{1}{B_1} - \frac{\alpha_1(1-Q_1)}{1-K_1^d/K_2^d}\right) \tag{15}$$

$$a_{33} = \frac{v_2\alpha_2}{K_2^d}\left(\frac{1}{B_2} - \frac{\alpha_2(1-Q_2)}{1-K_2^d/K_1^d}\right) \tag{16}$$

$$a_{12} = -v_1 Q_1 \alpha_1 / K_1^d \tag{17}$$

$$a_{13} = -v_2 Q_2 \alpha_2 / K_2^d \tag{18}$$

$$a_{23} = -\frac{\alpha_1\alpha_2 K_1^d/K_2^d}{(1-K_1^d/K_2^d)^2}\left(\frac{1}{K} - \frac{v_1}{K_1^d} - \frac{v_2}{K_2^d}\right) \tag{19}$$

where the Q_i are auxiliary constants given by

$$v_1 Q_1 = \frac{1-K_2^d/K}{1-K_2^d/K_1^d} \quad \text{and} \quad v_2 Q_2 = \frac{1-K_1^d/K}{1-K_1^d/K_2^d}. \tag{20}$$

Here, v_1 and v_2 are the volume fractions of each phase within an averaging volume of the composite. The one constant that has not yet been defined is the overall drained modulus $K = 1/a_{11}$ of the two-phase composite (the modulus defined in the quasi-static limit where the local fluid pressure throughout the composite is everywhere unchanged). It is through K that the a_{ij} potentially depend on the mesoscopic geometry of the two porous phases. However, a reasonable modeling choice when phase 2 is embedded within phase 1 is to simply take the geometry-independent harmonic mean $1/K = v_1/K_1^d + v_2/K_2^d$. Although this choice actually violates the Hashin-Shitrikman bounds (Hashin and Shtrikman, 1961) for truly isotropic media, it is nevertheless a reasonable choice for earth systems where the assumed isotropy is itself an approximation. This choice is also a particularly convenient one because it results in $Q_1 = Q_2 = 1$ as well as $a_{23} = 0$. All dependence on the fluid's bulk modulus is contained within the two Skempton's coefficients B_1 and B_2 and is thus restricted to a_{22} and a_{33}. In the quasi-static limit $\omega \to 0$ (fluid pressure everywhere uniform throughout the composite), equations (12) and (13) reduce to the known exact results of Berryman and Milton (1991) once equations (14)–(19) are employed.

Double-Porosity Transport

Pride and Berryman (2003b) obtain the internal transport coefficient γ of equation (9) as

$$\gamma(\omega) = \gamma_m\sqrt{1 - i\frac{\omega}{\omega_m}} \tag{21}$$

where the parameter γ_m that holds in the final stages of internal fluid-pressure equilibration is given by

$$\gamma_m = \frac{v_1 k_1}{\eta L_1^2}\left[1 + O(k_1/k_2)\right]. \tag{22}$$

Since the more compressible embedded phase 2 typically has a permeability much greater than the host phase 1, the $O(k_1/k_2)$ correction can be neglected. The transition frequency

ω_m corresponds to the onset of a high-frequency regime in which the fluid-pressure-diffusion penetration distance between the phases becomes small relative to the scale of the mesoscopic heterogeneity. It is given by

$$\omega_m = \frac{B_1 K_1^d}{\eta \alpha_1} \frac{k_1 (v_1 V/S)^2}{L_1^4} \left(1 + \sqrt{\frac{k_1 B_2 K_2^d \alpha_1}{k_2 B_1 K_1^d \alpha_2}} \right)^2 . \tag{23}$$

The length L_1 characterizes the average distance in phase 1 over which the fluid pressure gradient still exists in the final approach to equilibration and has the formal mathematical definition

$$L_1^2 = \frac{1}{V_1} \int_{\Omega_1} \Phi_1 \, dV = \frac{1}{V_1} \int_{\Omega_1} \nabla \Phi_1 \cdot \nabla \Phi_1 \, dV \tag{24}$$

where Ω_1 is the region of an averaging volume occupied by phase 1 and having a volume measure V_1. The potential Φ_1 has units of length squared and is a solution of an elliptic boundary-value problem that under conditions where the harmonic mean is a good approximation for the overall drained modulus and where the permeability ratio k_1/k_2 can be considered small, reduces to

$$\nabla^2 \Phi_1 = -1 \text{ in } \Omega_1, \tag{25}$$

$$\mathbf{n} \cdot \nabla \Phi_1 = 0 \text{ on } \partial E_1, \tag{26}$$

$$\Phi_1 = 0 \text{ on } \partial \Omega_{12}, \tag{27}$$

where ∂E_1 is the external surface of the averaging volume coincident with phase 1, and where $\partial \Omega_{12}$ is the internal interface separating phases 1 and 2. Multiplying equation (25) by Φ_1 and integrating over Ω_1, establishes that second integral of equation (24).

For complicated geometry, L_1 can only be determined numerically. For idealized geometries it can be analytically estimated. For example, if phase 2 is taken to be small spheres of radius a embedded within each sphere R of the composite, Pride and Berryman (2003b) obtain

$$L_1^2 = \frac{9}{14} R^2 \left[1 - \frac{7}{6} \frac{a}{R} + O(a^3/R^3) \right]. \tag{28}$$

The volume fraction v_2 of small spheres is then $v_2 = (a/R)^{1/3}$ which can be used to eliminate R since $R = a v_2^{-1/3}$. The other length parameter is the volume-to-surface ratio V/S where S is the area of $\partial \Omega_{12}$ in each volume V of composite. For the simple spherical-inclusion model, it is given by $V/S = R^3/(3a^2) = a v_2/3$.

The coefficient $G(\omega) - i\omega g(\omega)$ governing shear generally has a non-zero "viscosity" $g(\omega)$ associated with the mesoscopic fluid transport between the compressional lobes surrounding a sheared phase 2 inclusion. Both of the frequency functions $G(\omega)$ and $-\omega g(\omega)$ are real and are Hilbert transforms of each other. The frequency dependence of $g(\omega)$ was not modeled by Pride and Berryman (2003b). However, if the inclusions of phase 2 are taken to be spheres, then $g(\omega) = 0$ exactly and $G(\omega) = G$ is a constant that can be approximately modeled using a simple harmonic average $1/G = v_1/G_1 + v_2/G_2$ of the underlying shear moduli of each phase.

Finally, the dynamic permeability $k(\omega)$ to be used in the effective Biot theory can be modeled in several ways. Perhaps the simplest modeling choice when phase 2 is modeled as small inclusions embedded in phase 1 is to again take a harmonic average $1/k(\omega) = v_1/k_1(\omega) + v_2/k_2(\omega) \approx v_1/k_1(\omega)[1 + O(v_2 k_1/k_s)]$.

Phase Velocity and Attenuation

With all of the double-porosity coefficients now defined, the compressional phase velocity and attenuation may be determined by inserting a plane-wave solution into the effective single-porosity Biot equations [in the form (1)–(4)]. This gives the standard complex longtitudinal slowness s of Biot theory

$$s^2 = b \mp \sqrt{b^2 - \frac{\rho\tilde{\rho} - \rho_f^2}{MH - C^2}}, \tag{29}$$

where

$$b = \frac{\rho M + \tilde{\rho} H - 2\rho_f C}{2(MH - C^2)} \tag{30}$$

is simply an auxiliary parameter, and where H, C and M are the Biot (1962) poroelastic moduli defined in terms of the complex frequency-dependent parameters of equations (11)–(13) as

$$H = K_U + 4G/3 \tag{31}$$

$$C = BK_U \tag{32}$$

$$M = \frac{B^2}{1 - K_D/K_U} K_U. \tag{33}$$

The complex inertia $\tilde{\rho}$ corresponds to rewriting the relative flow resistance as an effective inertial effect

$$\tilde{\rho} = -\eta/[i\omega k(\omega)]. \tag{34}$$

Taking the minus sign in equation (29) gives an s having an imaginary part much smaller than the real part and that thus corresponds to the normal P-wave. Taking the positive sign gives an s with real and imaginary parts of roughly the same amplitude and that thus corresponds to the slow P-wave (a pure fluid-pressure diffusion across the seismic band of frequencies). We are only interested here in the properties of the normal P-wave.

The P-wave phase velocity v_p and the attenuation measure Q_p^{-1} are related to the complex slowness s as

$$v_p = 1/\mathrm{Re}\{s\} \tag{35}$$

$$Q_p^{-1} = \mathrm{Im}\{s\}/\mathrm{Re}\{s\}. \tag{36}$$

A Numerical Example

In Fig. 1, we give an example of Q_p^{-1} and v_p as determined using this double-porosity theory. The example models a consolidated sandstone containing pockets (small regions) where the

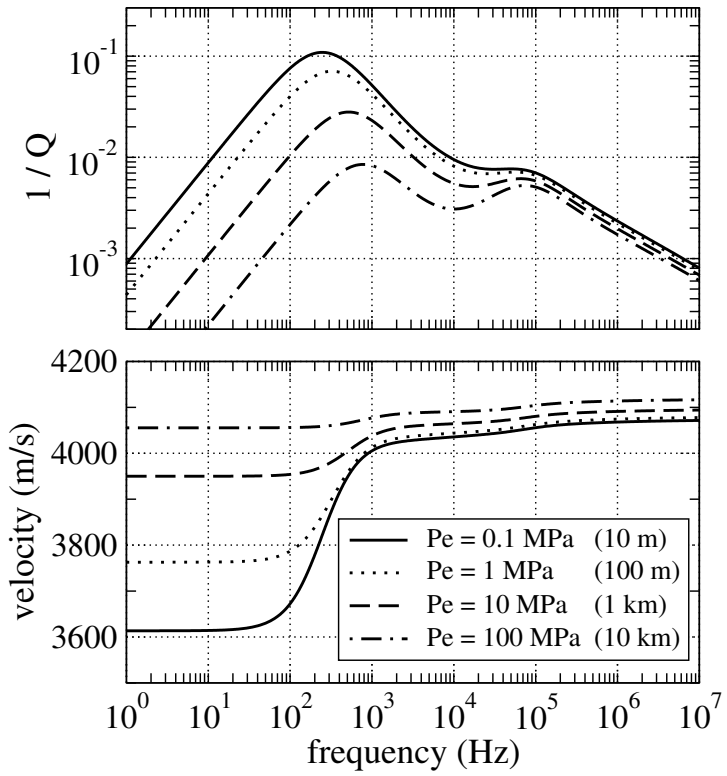

Figure 1: The attenuation and phase velocity of compressional waves in the double-porosity model of Pride and Berryman (2003a). The 5 cm embedded spheres of phase 2 have frame moduli (K_2^d and G_2) modeled using the modified Walton theory given in the appendix in which both K_2^d and G_2 vary strongly with the background effective pressure P_e (or overburden thickness). These spheres of porous continuum 2 were embedded into a phase 1 continuum modeled as a consolidated sandstone. jim3-QandVdp [NR]

grains are not cemented together. The embedded unconsolidated phase 2 is modeled as 5 cm radius spheres occupying 1.5% of the composite. The frame moduli of this relatively-compressible embedded material are determined using the modified Walton theory given in the Appendix. These moduli are functions of the background effective-stress level P_e. The host phase 1 is modeled as a consolidated sandstone (using $\phi_1 = 0.15$ and $c = 4$ in the model given in the appendix). The permeability of the two phases are taken as $k_1 = 10^{-14}$ m^2 and $k_2 = 10^{-12}$ m^2. The invariant peak near 10^5 Hz is that due to the Biot loss (fluid equilibration at the scale of the seismic wavelength) while the principal peak that changes with the effective pressure P_e is that due to mesoscopic-scale equilibration. Figure 1 demonstrates that small amounts of a relatively soft material embedded within a more consolidated rock is capable of producing the level of attenuation measured in field experiments.

The overall magnitude of attenuation in the model is controlled principally by the contrast of compressibilities between the two porous phases; the greater the contrast, the greater the mesoscopic fluid-pressure gradient and the greater the mesoscopic-flow intensity and associated attenuation. The relaxation frequency at which the mesoscopic loss per cycle is maximum is proportional to k_1/L_1^2. Below this relaxation frequency, Q^{-1} increases with frequency as $f\eta/k_1$. Thus, the permeability information in the double-porosity attenuation is principally in the frequency dependence of Q^{-1} and not in the overall magnitude of Q^{-1} and involves principally the permeability k_1 of the host phase and not the overall permeability of the composite. [See Berryman (1988) for a related discussion.] If phase 2 is well modeled as being small inclusions embedded in phase 1, then k_1 is controlling the overall permeability. If phase 2 corresponds to through going connected joints, then although $Q^{-1}(\omega)$ contains information about k_1, it does not contain information about the overall permeability which is being dominated by k_2 in this case.

PATCHY-SATURATION MODEL

Another important source of mesoscopic-scale heterogeneity is patchy fluid saturation. All natural hydrological processes by which one fluid non-miscibly invades a region initially occupied by another result in a patchy distribution of the two fluids. The patch sizes are distributed across the entire range of mesoscopic length scales and for many invasion scenarios are expected to be fractal. As a compressional wave squeezes such a material, the patches occupied by the less-compressible fluid will respond with a greater fluid-pressure change than the patches occupied by the more-compressible fluid. The two fluids will then equilibrate by the same type of mesoscopic flow already modeled in the double-porosity model.

An analysis almost identical to that of Pride and Berryman (2003a,b) can be carried out that leads to the same effective poroelastic moduli given by equations (11)–(13) but with different definitions of the a_{ij} constants and internal transport coefficient $\gamma(\omega)$. In the model, a single uniform porous frame is saturated by mesoscopic-scale patches of fluid 1 and fluid 2. We define porous phase 1 to be those regions (patches) occupied by the less mobile fluid and phase 2 the patches saturated by the more mobile fluid; i.e., by definition $\eta_1 > \eta_2$. This most often (but not necessarily) corresponds to $K_{f1} > K_{f2}$ and, therefore, to $B_1 > B_2$.

Johnson (2001) approached this problem using a different coarse-graining argument while starting from the same local physics (assuming, however, that the porous medium is a Gassmann mono-mineral material). The final undrained bulk modulus obtained by Johnson (2001) is identical to our model in the limits of high and low frequency and differs only negligibly in the transition range of frequencies where the flow in either model is not explicitly treated.

Patchy-Saturation a_{ij} Coefficients

To obtain the a_{ij} for the patchy-saturation model, we note that each patch has the same α and K. The poroelastic differences between patches is entirely due to B_1 being different than B_2. Upon volume averaging equation (3) and using $\nabla\cdot\mathbf{v} = \nabla\cdot\left(v_1\dot{\overline{\mathbf{u}}}_1\right) + \nabla\cdot\left(v_2\dot{\overline{\mathbf{u}}}_2\right)$, where an overline again denotes a volume average over the appropriate phase, and using the fact that the a_{ij} are defined in the extreme high-frequency limit where the fluids have no time to traverse the internal interface $\partial\Omega_{12}$ (i.e., the a_{ij} are defined under the condition that $\dot{\zeta}_{\text{int}} = 0$), one has

$$\nabla\cdot\mathbf{v} = -\frac{v_1}{K}\dot{\overline{p}}_{c1} - \frac{v_2}{K}\dot{\overline{p}}_{c2} + \frac{v_1\alpha}{K}\dot{\overline{p}}_{f1} + \frac{v_2\alpha}{K}\dot{\overline{p}}_{f2}, \tag{37}$$

$$\nabla\cdot\mathbf{q}_1 = \frac{v_1\alpha}{K}\dot{\overline{p}}_{c1} - \frac{v_1\alpha}{KB_1}\dot{\overline{p}}_{f1}, \tag{38}$$

$$\nabla\cdot\mathbf{q}_2 = \frac{v_2\alpha}{K}\dot{\overline{p}}_{c2} - \frac{v_2\alpha}{KB_2}\dot{\overline{p}}_{f2}. \tag{39}$$

The average confining pressures $\overline{p}_{ci}$ in each phase are not *a priori* known; however, they are necessarily linear functions of the three independent applied pressures of the theory $P_c(= v_1\overline{p}_{c1} + v_2\overline{p}_{c2})$, $\overline{p}_{f1}$, and $\overline{p}_{f2}$. It is straightforward to demonstrate that if and only if the average confining pressures take the form

$$v_1\dot{\overline{p}}_{c1} = v_1\dot{P}_c + \beta\dot{\overline{p}}_{f1} - \beta\dot{\overline{p}}_{f2} \tag{40}$$

$$v_2\dot{\overline{p}}_{c2} = v_2\dot{P}_c - \beta\dot{\overline{p}}_{f1} + \beta\dot{\overline{p}}_{f2}, \tag{41}$$

will equations (37)–(39) produce a_{ij} that satisfy the thermodynamic symmetry requirement of $a_{ij} = a_{ji}$ [i.e., these a_{ij} constants are all second derivatives of a strain-energy function as demonstrated by Pride and Berryman (2003a). Upon placing equations (40) and (41) into equations (37)–(39), we then have

$$a_{11} = 1/K \tag{42}$$

$$a_{22} = (-\beta + v_1/B_1)\alpha/K \tag{43}$$

$$a_{33} = (-\beta + v_2/B_2)\alpha/K \tag{44}$$

$$a_{12} = -v_1\alpha/K \tag{45}$$

$$a_{13} = -v_2\alpha/K \tag{46}$$

$$a_{23} = \beta\alpha/K \tag{47}$$

where β is a constant to be determined.

To obtain β, we note that in the high-frequency limit, each local patch of phase i is undrained and thus characterized by an undrained bulk modulus $K_i^u = K/(1-\alpha B_i)$ and a shear modulus G that is the same for all patches. In this limit, the usual laws of elasticity govern the response of this heterogeneous composite. Under these precise conditions (elasticity of an isotropic composite having uniform G and all heterogeneity confined to the bulk modulus which in the present case corresponds to K_i^u), the theorem of Hill (1963) applies, which states that the overall undrained-unrelaxed modulus of the composite K_H is given exactly by

$$\frac{1}{K_H + 4G/3} = \frac{v_1}{K_1^u + 4G/3} + \frac{v_2}{K_2^u + 4G/3}. \tag{48}$$

In terms of the a_{ij}, this same undrained-unrelaxed Hill modulus is given by

$$\frac{1}{K_H} = a_{11} + a_{12}\left(\frac{\delta p_{f1}}{\delta P_c}\right)_U + a_{13}\left(\frac{\delta p_{f2}}{\delta P_c}\right)_U \tag{49}$$

where, upon using $\nabla \cdot \mathbf{q}_i = 0$ and $\dot{\zeta}_{\text{int}} = 0$ in equation (8) and then using (42)–(47), the undrained-unrelaxed pressure ratios are

$$\left(\frac{\delta p_{f1}}{\delta P_c}\right)_U = \frac{\beta - v_1 v_2/B_2}{\beta(v_1/B_1 + v_2/B_2) - v_1 v_2/(B_1 B_2)} \tag{50}$$

$$\left(\frac{\delta p_{f2}}{\delta P_c}\right)_U = \frac{\beta - v_1 v_2/B_1}{\beta(v_1/B_1 + v_2/B_2) - v_1 v_2/(B_1 B_2)}. \tag{51}$$

Thus, after some algebra, equation (49) yields the exact result

$$\beta = v_1 v_2 \left(\frac{v_1}{B_2} + \frac{v_2}{B_1}\right)\left[\frac{\alpha - (1 - K/K_H)/(v_1 B_1 + v_2 B_2)}{\alpha - (1 - K/K_H)(v_1/B_1 + v_2/B_2)}\right] \tag{52}$$

with K_H given by equation (48). All the a_{ij} are now expressed in terms of known information.

Patchy-Saturation Transport

We next must address the internal fluid-pressure equilibration between the two phases with the goal of obtaining the internal transfer coefficient γ of equation (9). The mathematical definition of the rate of internal fluid transfer is

$$\dot{\zeta}_{\text{int}} = \frac{1}{V}\int_{\partial\Omega_{12}} \mathbf{n} \cdot \mathbf{Q}_1 \, dS \tag{53}$$

where V is the volume occupied by the composite. A possible concern in the patchy-saturation analysis is whether capillary effects at the local interface $\partial\Omega_{12}$ separating the two phases need to be allowed for.

Local continuity conditions on $\partial\Omega_{12}$

At the pore scale, the interface separating one fluid patch from the next is a series of meniscii. Roughness on the grain surfaces keeps the contact lines of these meniscii pinned to the grain surfaces. Pride and Flekkoy (1999) argue that the contact lines of an air-water meniscus will remain pinned for fluid-pressure changes less than roughly 10^4 Pa which correspond to the pressure range induced by linear seismic waves. So as a wave passes, the meniscii will bulge and change shape but will not migrate away. This makes the problem vastly more simple to analyze theoretically.

One porous-continuum boundary condition is that all fluid volume that locally enters the interface $\partial\Omega_{12}$ from one side, must exit the other side so that $\mathbf{n}\cdot\mathbf{Q}_1 = \mathbf{n}\cdot\mathbf{Q}_2\ (=\mathbf{n}\cdot\mathbf{Q})$. Another boundary condition is that the difference in the rate at which energy is entering and leaving the interface is entirely due to the work performed in changing the miniscii surface area. Before the wave arrives, each miniscus has an initial mean curvature H_o fixed by the static fluid pressures initially present; $p^o_{f1} - p^o_{f2} = \sigma H_o$ where σ is the surface tension. During wave passage, one can demonstrate (Pride and Flekkoy, 1999) that the mean curvature changes as $H = H_o + \epsilon H_1 + O(\epsilon^2)$ where H_1 is of the same order as H_o and where ϵ is a dimensionless number called the capillary number. The capillary number is defined $\epsilon = \eta|\mathbf{Q}|/\sigma$ where $|\mathbf{Q}|$ is some estimate of the wave-induced Darcy flux and that is thus bounded as the wave strain times phase velocity; i.e., $|\mathbf{Q}| < 10^{-3}$ m/s. For typical interfaces (like air and water), we have $\sigma > 10^{-2}$ Pa m and $\eta \approx 10^{-3}$ Pa s. Thus, for linear wave problems, $\epsilon \ll 10^{-4}$ and ϵ can be considered a very small number.

Writing the fluid pressures as $p_{fi} = p^o_{fi} + \delta p_{fi}$ and using the fact that $\mathbf{n}\cdot\mathbf{Q}$ is continuous, allows the conservation of energy at the interface to be expressed

$$\left[\mathbf{n}\cdot\left\{\boldsymbol{\tau}_i\cdot\dot{\mathbf{u}}_i - (p^o_{fi} + \delta p_{fi})\mathbf{Q}\right\}\right] = \sigma\,\mathbf{n}\cdot\mathbf{Q}H_o[1+O(\epsilon)]. \tag{54}$$

The brackets on the left-hand side deonte the jump in energy flux across the interface, while the right-hand side represents the rate at which work is performed in stretching the meniscii. Since conservation of momentum requires $\mathbf{n}\cdot\boldsymbol{\tau}$ to be continuous at the interface and since the assumption of the grains being welded together [or having an overburden effective pressure $(1-\phi)(\rho_s - \rho_f)gh$ acting on them that is greater than the wave stress] requires that $\dot{\mathbf{u}}$ is continuous, we obtain that to leading order in ϵ

$$\delta p_{f1} = \delta p_{f2} \tag{55}$$

along the interface $\partial\Omega_{12}$. This means that the fluid pressure equilibration can be modeled using the standard displacement-stress continuity conditions along $\partial\Omega_{12}$ that were also employed in the double-porosity analysis; i.e., capillary effects can be neglected. In what follows, the fluid pressures correspond to the changes induced by the wave and so we cease to explicitly write the "δ" in front of them.

Mesoscopic flow equations

To obtain the transport law $-i\omega\zeta_{\rm int} = \gamma(\omega)(\overline{p}_{f1} - \overline{p}_{f2})$, the mesoscopic flow is analyzed in the limits of low and high frequencies. These limits are then connected using a frequency function that respects causality constraints. The linear fluid response inside the patchy composite due to a seismic wave can always be resolved into two portions: (1) a vectorial response due to macroscopic fluid-pressure gradients across an averaging volume that generate a macroscopic Darcy flux $\mathbf{q}_i$ across each phase and that corresponds to the macroscopic conditions $\overline{p}_{fi} = 0$ and $\nabla\overline{p}_{fi} \neq 0$; and (2) a scalar response associated with internal fluid transfer and that corresponds to the macroscopic conditions $\overline{p}_{fi} \neq 0$ and $\nabla\overline{p}_{fi} = 0$. The macroscopic isotropy of the composite guarantees that there is no cross-coupling between the vectorial transport $\mathbf{q}_i$ and the scalar transport $\dot{\zeta}_{\rm int}$ within each sample.

The mesoscopic flow problem that defines $\dot{\zeta}_{\rm int}$ is the internal equilibration of fluid pressure between the patches when a confining pressure ΔP has been applied to a sealed sample of the composite. Having the external surface sealed is equivalent to the required macroscopic constraint that $\nabla\overline{p}_{fi} = 0$. Upon taking the divergence of (2) and using equation (3), the diffusion problem controling the mesoscopic flow becomes

$$\frac{k}{\eta_i}\nabla^2 p_{fi} + i\omega\frac{\alpha}{KB_i}p_{fi} = i\omega\frac{\alpha}{K}p_{ci} \quad \text{in } \Omega_i, \tag{56}$$

$$\left[p_{fi}\right] \text{ and } \left[\mathbf{n}\cdot\nabla p_{fi}\right] = 0 \quad \text{on } \partial\Omega_{12}, \tag{57}$$

$$\mathbf{n}\cdot\nabla p_{fi} = 0 \quad \text{on } \partial E_i, \tag{58}$$

where Ω_i is the region that each phase occupies within the averaging volume, ∂E_i is that portion of the external surface of the averaging volume that is in contact with phase i, and the brackets in equation (57) again denote jumps across the interface. One also needs to insert equations (3) and (4) into (1) to obtain a second-order partial-differential equation for the displacements $\mathbf{u}_i$. In general, the local confining pressures p_{ci} are determined using

$$p_{ci} = -K\nabla\cdot\mathbf{u}_i + \alpha p_{fi} \tag{59}$$

once the displacements $\mathbf{u}_i$ are known.

Low-frequency limit of $\gamma(\omega)$

As $\omega \to 0$, one can represent the local fields as asymptotic series in the small parameter $-i\omega$

$$p_{fi} = p_{fi}^{(0)} - i\omega p_{fi}^{(1)} + O(\omega^2), \tag{60}$$

$$p_{ci} = p_{ci}^{(0)} - i\omega p_{ci}^{(1)} + O(\omega^2), \tag{61}$$

and equivalently for $\mathbf{u}_i$. The zeroth-order response corresponds to uniform fluid pressure in the pores and is therfore given by $p_{c1}^{(0)} = p_{c2}^{(0)} = \Delta P$ and

$$\frac{\overline{p}_{fi}^{(0)}}{\Delta P} = B_o = -\frac{a_{12}+a_{13}}{a_{22}+2a_{23}+a_{33}} = \frac{1}{v_1/B_1 + v_2/B_2} \tag{62}$$

where the patchy-saturation a_{ij} have been employed. The fact that the quasi-static Skempton's coefficient in the patchy-saturation model is exactly the harmonic average of the constituents B_i is equivalent to saying that at low frequencies, the fluid bulk modulus is given by $1/K_f = v_1/K_{f1} + v_2/K_{f2}$. The quasi-static response is thus completely independent of the spatial geometry of the fluid patches; it depends only on the volume fractions occupied by the patches.

The leading order correction to uniform fluid pressure is then controlled by the boundary-value problem

$$\frac{Kk}{\alpha\eta_1}\nabla^2 p_{f2}^{(1)} = \frac{\eta_2}{\eta_1}\left(1-\frac{B_o}{B_2}\right)\Delta P \quad \text{in } \Omega_2, \tag{63}$$

$$\frac{Kk}{\alpha\eta_1}\nabla^2 p_{f1}^{(1)} = \left(1-\frac{B_o}{B_1}\right)\Delta P \quad \text{in } \Omega_1, \tag{64}$$

$$p_{f1}^{(1)} = p_{f2}^{(1)} \quad \text{on } \partial\Omega_{12} \tag{65}$$

$$\mathbf{n}\cdot\nabla p_{f2}^{(1)} = \frac{\eta_2}{\eta_1}\mathbf{n}\cdot\nabla p_{f1}^{(1)} \quad \text{on } \partial\Omega_{12} \tag{66}$$

$$\mathbf{n}\cdot\nabla p_{fi}^{(1)} = 0 \quad \text{on } \partial E_i. \tag{67}$$

It is now assumed that for patchy-saturation cases of interest (air/water or water/oil), the ratio η_2/η_1 can be considered small. To leading order in η_2/η_1, equations (63), (66), and (67) require that $p_{f2}^{(1)}(\mathbf{r}) = \overline{p}_{f2}^{(1)}$ (a spatial constant). The fluid pressure in phase 1 is now rewritten as

$$p_{f1}^{(1)}(\mathbf{r}) = \overline{p}_{f2}^{(1)} - \frac{\eta_1\alpha}{kK}\left(1-\frac{B_o}{B_1}\right)\Delta P\,\Phi_1(\mathbf{r}) \tag{68}$$

where, from equations (64), (65) and (67) and to leading order in η_2/η_1, the potential Φ_1 is the solution of the same elliptic boundary-value problem (25)–(27) given earlier.

Upon averaging (68) over all of Ω_1, the leading order in $-i\omega$ difference in the average fluid pressures can be written

$$\frac{\overline{p}_{f1}-\overline{p}_{f2}}{\Delta P} = -i\omega\left(\frac{\overline{p}_{f1}^{(1)}-\overline{p}_{f2}^{(1)}}{\Delta P}\right) = i\omega\frac{\eta_1\alpha}{kK}\left(1-\frac{B_o}{B_1}\right)L_1^2 \tag{69}$$

where L_1 is again the length defined by equation (24).

To connect this fluid-pressure difference to the increment $\dot{\zeta}_{\text{int}}$ we use the divergence theorem and the no-flow boundary condition on ∂E_i to write equation (53) as

$$-i\omega\zeta_{\text{int}} = \frac{i\omega}{V}\frac{k}{\eta}\int_{\partial\Omega_{12}}\mathbf{n}\cdot\nabla p_{f1}^{(1)}\,dS = i\omega v_1\frac{\alpha}{K}\left(1-\frac{B_o}{B_1}\right)\Delta P. \tag{70}$$

Replacing ΔP with $\overline{p}_{f1}-\overline{p}_{f2}$ using equation (69) then gives the desired law $-i\omega\zeta_{\text{int}} = \gamma_p(\overline{p}_{f1}-\overline{p}_{f2})$ with

$$\gamma_p = \frac{v_1 k}{\eta_1 L_1^2}\left[1+O\left(\frac{\eta_2}{\eta_1}\right)\right]. \tag{71}$$

being the low-frequency limit of interest.

High-frequency limit of $\gamma(\omega)$

It has already been commented that in the extreme high-frequency limit where each patch behaves as if it were sealed to flow ($\dot{\zeta}_{\rm int} = 0$), the theory of Hill (1963) applies. Hill demonstrated, among other things, that when each isotropic patch has the same shear modulus, the volumetric deformation within each patch is a spatial constant. The fluid pressure response in this limit p_{fi}^{∞} is thus a uniform spatial constant throughout each phase except in a vanishingly small neighborhood of the interface $\partial\Omega_{12}$ where equilibration is attempting to take place. The small amount of fluid-pressure penetration that is occuring across $\partial\Omega_{12}$ can be locally modeled as a one-dimensional process normal to the interface.

Using the coordinate x to measure linear distance normal to the interface (and into phase 1), one has that equation (56) is satisfied by

$$p_{f1} = p_{f1}^{\infty} + C_1 e^{i\sqrt{i\omega/D_1}\,x} \tag{72}$$

$$p_{f2} = p_{f2}^{\infty} + C_2 e^{-i\sqrt{i\omega/D_1}\,x} \tag{73}$$

where the diffusivities are defined $D_i = kKB_i/(\eta_i\alpha)$. The constants C_i are found from the continuity conditions (57) to be

$$C_1 = \frac{-1}{1+\sqrt{\eta_2 B_2/(\eta_1 B_1)}}(p_{f1}^{\infty} - p_{f2}^{\infty}) \tag{74}$$

$$C_2 = \frac{\sqrt{\eta_2 B_2/(\eta_1 B_1)}}{1+\sqrt{\eta_2 B_2/(\eta_1 B_1)}}(p_{f1}^{\infty} - p_{f2}^{\infty}). \tag{75}$$

Although not actually needed here, we have that $p_{fi}^{\infty} = B_i p_{ci}$ where the uniform confining pressure of each patch is given by equations (40) and (41) so that the fluid pressure difference between the phases goes as

$$\frac{p_{f1}^{\infty} - p_{f2}^{\infty}}{\Delta P} = \frac{B_1 - B_2}{1 - \beta(B_1/v_1 + B_2/v_2)}. \tag{76}$$

This equation is exactly the difference between equations (50) and (51). Because the penetration distance $\sqrt{D_i/\omega}$ vanishes at high-frequencies, we may state that to leading order in the high-frequency limit, $\overline{p}_{f1} - \overline{p}_{f2} = p_{f1}^{\infty} - p_{f2}^{\infty}$.

To obtain the high-frequency limit of the transport coefficient $\gamma(\omega)$, we use the definition (53) of the internal transport (note that $-\mathbf{n}\cdot\nabla p_{f1} = \partial p_{f1}/\partial x$)

$$-i\omega\zeta_{\rm int} = \frac{1}{V}\frac{k}{\eta_1}\int_{\partial\Omega_{12}} \frac{\partial p_{f1}}{\partial x}\, dS \tag{77}$$

along with equations (72) and (74). The result is

$$\lim_{\omega\to\infty}\gamma(\omega) = i^{3/2}\sqrt{\omega}\frac{S}{V}\left(\frac{\sqrt{k\alpha/(\eta_1 B_1 K)}}{1+\sqrt{\eta_2 B_2/(\eta_1 B_1)}}\right). \tag{78}$$

Here, S is again the area of $\partial\Omega_{12}$ contained within a volume V of the patchy composite.

Full-model for $\gamma(\omega)$

The high- and low-frequency limits of γ are then connected by a simple frequency function to obtain the final model

$$\gamma(\omega) = \gamma_p \sqrt{1 - i\omega/\omega_p} \tag{79}$$

where the transition frequency ω_p is defined

$$\omega_p = \frac{B_1 K}{\eta_1 \alpha} \frac{k(v_1 V/S)^2}{L_1^4} \left(1 + \sqrt{\frac{\eta_2 B_2}{\eta_1 B_1}}\right)^2 \tag{80}$$

and where $\gamma_p = v_1 k/(\eta_1 L_1^2)$. Equation (79) has a single singularity (a branch point) at $\omega = -i\omega_p$. Causality requires that with an $e^{-i\omega t}$ time dependence, all singularities and zeroes of a transport coefficient like $\gamma(\omega)$ must reside in the lower-half complex ω plane. Equation (79) satisfies this physically important constraint.

Patchy-Saturation Modeling Choices

To use the patchy-saturation model, appropriate values for the two geometric terms L_1 and V/S must be specified. Immiscible fluid distributions in the earth have very complicated geometries since they arise from slow flow that often produces fractal patch distributions. In particular, analytical solutions of the boundary-value problem (25)–(27) that defines L_1 for such real-earth situations are impossible. Recall that L_1 is a characteristic length of phase 1 (the phase having the smaller fluid mobility k/η) that defines the distance overwhich the fluid-pressure gradient is defined during the final stages of equilibration. For complicated geometries it may either be numerically determined, guessed at, or treated as a target parameter for a full-waveform inversion of seismic data. In the numerical examples that follow, we simply assume that the individual patches correspond to disconnected spheres for which simple analytical results are available for L_1 and V/S.

If we consider phase 2 (porous continuum saturated by the less viscous fluid) to be in the form of spheres of radius a embedded within each radius R sphere of the two-phase composite, then $v_2 = (a/R)^3$, $V/S = av_2/3$, and $L_1^2 = 9v_2^{-2/3}a^2/14[1 - 7v_2^{1/3}/6]$. This model is particularly appropriate when $v_2 \ll v_1$. Since the fluid 2 patches are disconnected, the definitions (11)–(13) of the effective poroelastic moduli again hold. Further, fluid 2 may be taken to be immobile relative to the framework of grains in the wavelength-scale Biot equilibration so that the inertial properties of equations (29) and (30) are identified as $\rho_f = \rho_{f1}$, $\rho = (1-\phi)\rho_s + \phi(v_1\rho_{f1} + v_2\rho_{f2})$ and $\tilde{\rho} = -\eta_1/(i\omega k)$.

In situations where it is more appropriate to treat fluid 1 (the more viscous fluid) as occuping disconnected patches (e.g., when $v_1 \ll v_2$), the effective poroelastic moduli are defined by replacing 2 with 3 (and 3 with 2) in the subscripts of equations (11)–(13). Again assuming the phase-1 patches to be spheres of radius a embedded within radius R sphere of the two-phase composite, we have that $v_1 = (a/R)^3$ and $V/S = av_1/3$. The elliptic boundary-value problem (25)–(27) can be solved in this case to give $L_1^2 = a^2/15$. Furthermore, the effective inertial

coefficients in the Biot theory are defined $\rho_f = \rho_{f2}$, $\rho = (1-\phi)\rho_s + \phi(v_1\rho_{f1} + v_2\rho_{f2})$, and $\tilde{\rho} = -\eta_2/(i\omega k)$.

In situations where both phases form continuous paths across each averaging volume, it is best to determine the attenuation and phase velocity by seeking the plane longtitudinal-wave solution of non-reduced "double-porosity" governing equations of the form (6)–(10). However, this approach is not pursued here. We conclude by noting that if the embedded fluid is fractally distributed, the lengths L_1 will remain finite while $(V/S)/L_1 \to 0$ as the fractal surface area S becomes large (however, V/S never reaches zero because the fractality has a small-scale cutoff fixed by the grain size of the material).

Numerical Examples

In Fig. 2, we compare the prediction of Johnson (2001) for K_U to our own for a consolidated sandstone (frame properties as determined in the Appendix with $k = 100$ mD, $c = 10$, $\phi = 0.20$) in which phase 1 is saturated with water and phase 2 is taken to be spherical regions saturated with air. The two estimates have identical asymptotic dependence in both the limits of high and low frequencies. In the cross-over range, the physics is not precisely modeled in either approach. However, even in the cross-over range, the differences in the two models is slight.

Figure 3 gives the P-velocity and attenuation for a model in which the frame properties correspond to $k = 10$ mD, $c = 15$, and $\phi = 0.15$. Phase 2 is saturated by air and is taken to be isolated spheres of radius $a = 1$ cm. Phase 1 is saturated with water. The volume fraction v_2 occupied by these 1 cm spheres of gas is as shown in the figure. Even tiny amounts of gas saturation yields rather large amounts of attenuation and dispersion.

SQUIRT-FLOW MODEL

Laboratory samples of consolidated rock often have broken grain contacts and/or microcracks in the grains. Much of this damage occurs as the rock is brought from depth to the surface. Since diagenetic processes in a sedimentary basin tend to cement microcracks and grain contacts, it is uncertain whether *in situ* rocks have significant numbers of open microcracks. Nonetheless, when such grain-scale damage is present, as it always is in laboratory rock samples at ambient pressures, the fluid-pressure response in the microcracks will be greater than in the principal porespace when the rock is compressed by a P-wave. The resulting flow from crack to pore is called "squirt flow" and Dvorkin *et al.* (1995) have obtained a quantitative model for fully-saturated rocks.

In the squirt model of Dvorkin *et al.* (1995), the grains of a porous material are themselves allowed to have porosity in the form of microcracks. The effect of each broken grain contact is taken as equivalent to a microcrack in a grain. The number of such microcracks per grain is thus limited by the coordination number of the packing and so the total porosity contribution coming from the grains is always negligible compared to the porosity of the main porespace.

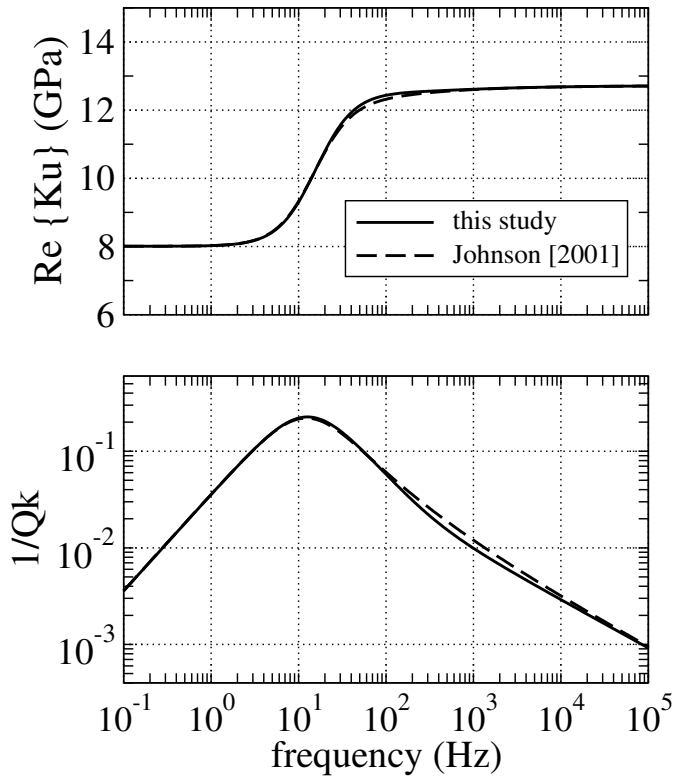

Figure 2: The undrained bulk modulus $K_U(\omega)$ in both the patchy-saturation model presented in this chapter and the model of Johnson (2001). The top graph is $\mathrm{Re}\{K_U\}$ while the bottom graph is $Q_K^{-1} = -2\mathrm{Im}\{K_U\}/\mathrm{Re}\{K_U\}$. The physical model is 10 cm spherical air pockets embedded within a water-saturated region. The volume fraction of gas saturated rock is 3% in this example. The properties of the rock correspond to a 100 mD consolidated sandstone. jim3-pridejohn [NR]

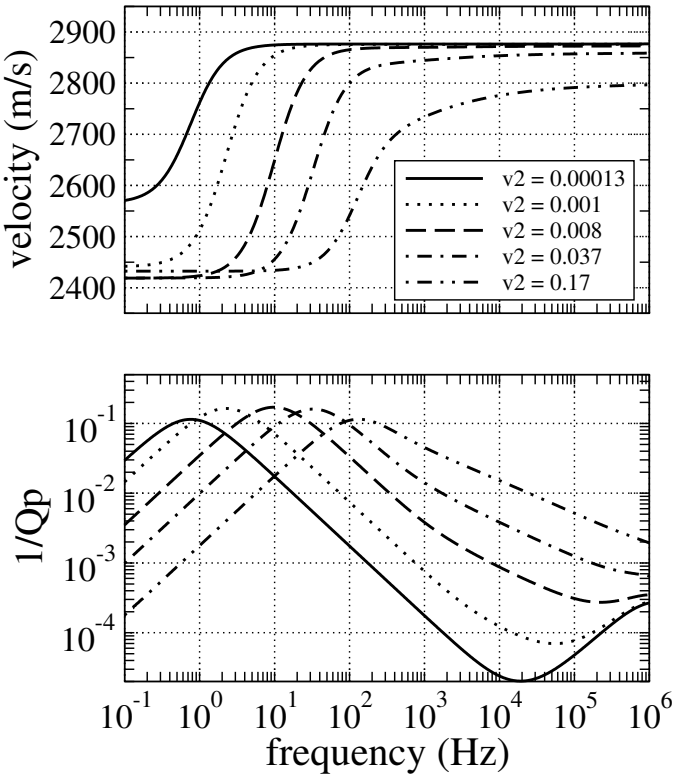

Figure 3: The P-wave velocity and attenuation of a sandstone saturated with water and containing small spherical pockets of gas having radius 1 cm and occuping a fraction of the volume v_2 as shown. jim3-vq [NR]

Our modeling of squirt is also based on this idea but we use the double-porosity framework of the previous sections. Phase 1 is now defined to be the pure fluid within the main porespace of a sample and is characterized elastically by the single modulus K_f (fluid bulk modulus). Phase 2 is taken to be the porous (i.e., cracked) grains and characterized by the poroelastic constants K_2^d (the drained modulus of an isolated porous grain), α_2 (the Biot-Willis constant of an isolated grain), and B_2 (Skempton's coefficient of an isolated grain) as well as by a permeability k_2. The overall composite of porous grains (phase 2) packed together within the fluid (phase 1) has two distinct properties of its own that must be specified; an overall drained modulus K, and an overall permeability k associated with flow through the main porespace. The volume fractions occupied by each phase are again denoted v_i where $v_1 = \phi$ is the porosity associated with the main porespace.

The theoretical approach is to again obtain the average fluid response in each of these two phases and then to make an effective Biot theory by saying that the fluid within the grains cannot communicate directly with the outside world; i.e., the fluid in the grains can only communicate with the main pores. Equations (11)–(12) again define the effective poroelastic moduli in the squirt model and we need only determine the a_{ij} constants and internal transport coefficient $\gamma(\omega)$ that are appropriate to squirt.

Squirt a_{ij} Coefficients

To obtain the a_{ij} coefficients in the squirt model, we first note that these coefficients are defined under conditions where $\dot{\zeta}_{\text{int}} = 0$ (no fluid passing between the porous grains and the principal porespace). Under these conditions, the rate of fluid depletion $\nabla \cdot \mathbf{q}_1$ of a sample (rate of fluid volume being extruded from the principal pore space via the exterior sample surface as normalized by the sample volume) is due to the difference between the rate of dilatation of the principal porespace (denoted here as $\dot{e}_1$) and the rate at which fluid in the pores is dilating $-\dot{\overline{p}}_{f1}/K_f$. If we also perform a volume average of equation (3) over the porous grain space and use the notation that $v_2\dot{e}_2 = \nabla \cdot (v_2 \dot{\overline{\mathbf{u}}}_2)$ we obtain the following three equations

$$\nabla \cdot \mathbf{q}_1 = v_1\dot{e}_1 + \frac{v_1}{K_f}\dot{\overline{p}}_{f1} \tag{81}$$

$$\nabla \cdot \mathbf{q}_2 = \frac{v_2\alpha_2}{K_2^d}\dot{\overline{p}}_{c2} - \frac{v_2\alpha_2}{B_2K_2^d}\dot{\overline{p}}_{f2} \tag{82}$$

$$v_2\dot{e}_2 = \frac{v_2}{K_2^d}\dot{\overline{p}}_{c2} - \frac{v_2\alpha_2}{K_2^d}\dot{\overline{p}}_{f2}. \tag{83}$$

The macroscopic dilatation of interest is $\nabla \cdot \mathbf{v} = v_1\dot{e}_1 + v_2\dot{e}_2$. In order to obtain the macroscopic compressibility laws for porous-grain/principal-porespace composite, we introduce linear response laws of the form

$$\dot{\overline{p}}_{c2} = a_1\dot{P}_c + a_2\dot{\overline{p}}_{f1} + a_3\dot{\overline{p}}_{f2} \tag{84}$$

$$\dot{e}_1 = b_1\dot{P}_c + b_2\dot{\overline{p}}_{f1} + b_3\dot{\overline{p}}_{f2} \tag{85}$$

where the a_i and b_i must be found. We note immediately that from the definition $\dot{\overline{P}}_c = v_1\dot{\overline{p}}_{f1} + v_2\dot{\overline{p}}_{c2}$ one has

$$0 = (1 - v_2a_1)\dot{P}_c - (v_1 + v_2a_2)\dot{\overline{p}}_{f1} - v_2a_3\dot{\overline{p}}_{f2} \tag{86}$$

which must hold true for any variation of the independent pressure variables so that $a_1 = 1/v_2$, $a_2 = -v_1/v_2$, $a_3 = 0$.

To obtain the b_i, we now combine the above into the macroscopic laws

$$-\nabla\cdot\mathbf{v} = \left[v_1 b_1 + \frac{1}{K_2^d}\right]\dot{P}_c + \left[v_1 b_2 - \frac{v_1}{K_2^d}\right]\dot{\overline{p}}_{f1} + \left[v_1 b_3 - \frac{v_2\alpha_2}{K_2^d}\right]\dot{\overline{p}}_{f2} \tag{87}$$

$$-\nabla\cdot\mathbf{q}_1 = -v_1 b_1 \dot{P}_c - \left[v_1 b_2 - \frac{v_1}{K_f}\right]\dot{\overline{p}}_{f1} - v_1 b_3 \dot{\overline{p}}_{f2} \tag{88}$$

$$-\nabla\cdot\mathbf{q}_2 = \frac{-\alpha_2}{K_2^d}\dot{P}_c + \frac{v_1\alpha_2}{K_2^d}\dot{\overline{p}}_{f1} + \frac{v_2\alpha_2}{K_2^d B_2}\dot{\overline{p}}_{f2} \tag{89}$$

and use the fact that the coefficients of the matrix must be symmetric ($a_{ij} = a_{ji}$). With $a_{11} = 1/K$ corresponding to the overall drained frame modulus of the composite (to be independently specified), we obtain $v_1 b_1 = 1/K - 1/K_2^d$, $v_1 b_2 = -1/K + (1+v_1)/K_2^d$, and $b_3 = -\alpha_2/K_2^d$. The final a_{ij} coefficients are exactly

$$a_{11} = 1/K \tag{90}$$

$$a_{22} = 1/K - (1+v_1)/K_2^d + v_1/K_f \tag{91}$$

$$a_{33} = \frac{v_2\alpha_2}{B_2 K_2^d} \tag{92}$$

$$a_{12} = -1/K + 1/K_2^d \tag{93}$$

$$a_{13} = -\alpha_2/K_2^d \tag{94}$$

$$a_{23} = v_1\alpha_2/K_2^d. \tag{95}$$

Reasonable models for K and K_2^d will be discussed shortly.

Squirt Transport

We next must obtain the coefficient $\gamma(\omega)$ in the mesoscopic transport law $-i\omega\zeta_{\text{int}} = \gamma(\omega)(\overline{p}_{f1} - \overline{p}_{f2})$. Again, the approach is to first obtain the limiting behaviour at low and high frequencies and then to connect the two limits by a simple function.

The fluid response in phase 1 (the principal porespace) is governed by the Navier-Stokes equation $-\nabla p_{f1} + \eta\nabla^2\mathbf{v}_1 = -i\omega\rho_f\mathbf{v}_1$ and the compressibility law $K_f\nabla\cdot\mathbf{v}_1 = i\omega p_{f1}$ where $\mathbf{v}_1$ is the local fluid velocity in the pores. Since for all frequencies of interest we have that $\omega \ll K_f/\eta$ (note that $K_f/\eta \approx 10^{12}$ s^{-1} for liquids and 10^{10} s^{-1} for gases), the fluid pressure in phase 1 is governed by the wave equation

$$\nabla^2 p_{f1} + \omega^2\frac{\rho_f}{K_f}p_{f1} = 0 \tag{96}$$

and since the acoustic wavelength in the fluid is always much greater than the grain sizes, the fluid pressure in the principal porespace satisfies $p_{f1}(\mathbf{r}) = \overline{p}_{f1}$ (a spatial constant) at all frequencies.

The focus, then, is on determining the flow and fluid pressure within the cracked grains (phase 2) that is governed by the local porous-continuum laws $\mathbf{Q}_2 = -(k_2/\eta)\nabla p_{f2}$ and

$$\frac{k_2}{\eta}\nabla p_{f2} + i\omega\frac{\alpha_2}{K_2^d B_2} p_{f2} = -i\omega\frac{\alpha_2}{K_2^d} p_{c2} \tag{97}$$

where $p_{c2} = -K_2^d \nabla\cdot\mathbf{u}_2 + \alpha_2 p_{f2}$. This deformation and pressure change is excited by applying a uniform normal stress $-\Delta P\mathbf{n}$ to the surface of the averaging volume with the fluid pressure satisfying the boundary conditions $\mathbf{n}\cdot\nabla p_{f2}(\mathbf{r}) = 0$ on ∂E_2 and $p_{f2}(\mathbf{r}) = \overline{p}_{f1}$ on $\partial\Omega_{12}$.

Low-frequency limit of $\gamma(\omega)$

The fluid pressure and confining pressure in the grains can again be developed as asymptotic series in $-i\omega$ [as in equations (60)–(61)]. The zero-order response corresponds to the static limit in which the fluid pressure is everywhere the same and given by $p_{f2}^{(0)} = \overline{p}_{f1} = B_o\Delta P$ with $B_o = -(a_{12}+a_{13})/(a_{22}+2a_{23}+a_{33})$ and with the a_{ij} as given by equations (90)–(95). The detailed result for B_o can be expressed

$$\begin{aligned}\frac{1/K - (1-\alpha_2)/K_2^d}{B_o} &= \frac{1}{K} - \frac{(1-\alpha_2)}{K_2^d} \\ &+ v_1\left[\frac{1}{K_f} - \frac{(1-\alpha_2)}{K_2^d}\right] + v_2\frac{\alpha_2}{K_2^d}\left[\frac{1}{B_2} - 1\right]\end{aligned} \tag{98}$$

which reduces to the standard Gassmann expression given in the appendix (with a total porosity given by $v_1 + \phi_2 v_2$) when B_2 and α_2 are themselves given by the Gassmann expressions. In this same zero-order limit, the undrained bulk modulus is defined as $1/K_o^u = a_{11} + (a_{12}+a_{13})B_o$ which also reduces to the standard Gassmann expression when B_2 and α_2 are themselves given by Gassmann expressions.

The leading-order in $-i\omega$ correction to uniform fluid pressure is thus governed by the problem

$$\nabla^2 p_{f2}^{(1)} = \frac{\eta\alpha_2}{k_2 K_2^d} p_{c2}^{(0)} \tag{99}$$

$$\mathbf{n}\cdot\nabla p_{f2}^{(1)} = 0 \quad \text{on} \quad \partial E_2 \tag{100}$$

$$p_{f2}^{(1)} = 0 \quad \text{on} \quad \partial\Omega_{12}. \tag{101}$$

Here, $p_{c2}^{(0)}$ is the local confining pressure in the grain space in the static limit that can be written $p_{c2}^{(0)}(\mathbf{r}) = \overline{p}_{c2}^{(0)} + \delta P(\mathbf{r})$. The average static confining pressure throughout the grains is determined from equation (84) with $P_c = \Delta P$ and $p_{f2} = p_{f1} = B_o\Delta P$ to yield

$$\overline{p}_{c2}^{(0)} = \frac{(1 - v_1 B_o)}{v_2}\Delta P. \tag{102}$$

The deviations $\delta P(\mathbf{r})$ thus volume integrate to zero $\overline{\delta P} = 0$ and are formally defined

$$\delta P(\mathbf{r}) = -\left(\frac{1-(v_1+v_2\alpha_2)B_o}{v_2}\right)\Delta P - \frac{K_2^d}{\alpha_2}\nabla\cdot\mathbf{u}^{(0)}(\mathbf{r}). \tag{103}$$

The local perturbations $\delta P(\mathbf{r})$ are thus highly sensitive to the detailed nature of the grain packing and grain geometry. Fortunately, these perturbations do not play an important role in the theory.

The fluid pressure in the grains is now written in the scaled form

$$p_{f2}^{(1)}(\mathbf{r}) = -\frac{\eta\alpha_2(1-v_1B_o)}{v_2k_2K_s^d}\Delta P\,\Phi(\mathbf{r}) \tag{104}$$

where the potential $\Phi(\mathbf{r})$ is independent of ΔP and is a solution of the elliptic problem

$$\nabla^2\Phi(\mathbf{r}) = -1 - \frac{v_2}{1-v_1B_o}\frac{\delta P(\mathbf{r})}{\Delta P} \tag{105}$$

$$\mathbf{n}\cdot\nabla\Phi = 0 \quad \text{on } \partial E_2 \tag{106}$$

$$\Phi = 0 \quad \text{on } \partial\Omega_{12}. \tag{107}$$

To leading-order in $-i\omega$, an average of equation (104) gives

$$\overline{p}_{f1} - \overline{p}_{f2} = i\omega\overline{p}_{f2}^{(1)} + O(\omega^2) \tag{108}$$

$$= -i\omega\frac{\eta\alpha_2(1-v_1B_o)}{v_2k_2K_s^d}L_2^2\Delta P + O(\omega^2) \tag{109}$$

where the squared length L_2^2 is defined

$$L_2^2 = \overline{\Phi} = \overline{\Phi}_o\left[1 + \frac{v_2}{1-v_1B_o}\frac{\overline{\Phi_o\delta P}}{\overline{\Phi}_o\Delta P}\right] \tag{110}$$

with overlines denoting volume averages over the grain space and with the potential Φ_o defined as the solution of

$$\nabla^2\Phi_o = -1 \tag{111}$$

$$\mathbf{n}\cdot\nabla\Phi_o = 0 \quad \text{on } \partial E_2 \tag{112}$$

$$\Phi_o = 0 \quad \text{on } \partial\Omega_{12}. \tag{113}$$

Although it is not generally true that $\overline{\Phi_o\delta P} = 0$ for all grain geometries, we nonetheless expect this integral to be small because Φ_o is a smooth function and $\overline{\delta P} = 0$. The local perturbations in the static confining pressure $\delta P(\mathbf{r})$ require a solution of the static displacements throughout the entire grain space—a daunting numerical task. Whenever the length L_2 needs to be estimated, such as in the numerical results that follow, our approach is to simply use the reasonable approximation that $L_2^2 = \overline{\Phi}_o$.

Last, from the definition $\dot{\zeta}_{\rm int}$ of the internal transfer we have that to leading order in $-i\omega$

$$-i\omega\zeta_{\rm int} = \frac{i\omega k_2}{V\eta}\int_{\partial\Omega_{12}} \mathbf{n}\cdot\nabla p_{f2}^{(1)} \tag{114}$$

$$= \frac{-i\omega k_2}{V\eta}\int_{\Omega_2} \nabla^2 p_{f2}^{(1)} = -i\omega\frac{\alpha_2}{K_2^d} v_2 \overline{p}_{c2}^{(0)} \tag{115}$$

$$= \frac{v_2 k_2}{\eta L_2^2}(\overline{p}_{f1} - \overline{p}_{f2}). \tag{116}$$

The normal $\mathbf{n}$ in equation (114) is outward to phase 1 which accounts for the sign change in equation(115). Note as well that equation (115) is a volume average of equation (99) while equation (116) follows from equations (102) and (109). The desired limit is thus $\lim_{\omega\to 0}\gamma(\omega) = \gamma_{sq} = v_2 k_2/(\eta L_2^2)$.

High-frequency limit of $\gamma(\omega)$

In the extreme high-frequency limit, the fluid has no time to significantly escape from the porous grains (phase 2) and enter the main porespace (phase 1). As such, the fluid pressure distribution in each phase is reasonably modeled as

$$p_{f1}(\mathbf{r}) = B_1^\infty \Delta P \tag{117}$$

$$p_{f2}(\mathbf{r}) = B_2^\infty \Delta P + C_2 \Delta P e^{-i^{3/2}\sqrt{\omega/D_2}\,x} \tag{118}$$

where x is again a local coordinate measuring distance normal to the interface $\partial\Omega_{12}$ and where D_2 is the fluid-pressure diffusivity within the porous grains that is given by $D_2 = k_2 K_2^d B_2/(\eta\alpha_2)$. In reality, the local confining pressure $p_{c2}(\mathbf{r})$ throughout the grains has spatial fluctuations about the average value and we have made the approximation that $B_2 p_{c2}(\mathbf{r}) \approx B_2^\infty \Delta P$ = the average fluid pressure throughout the grain space. It is easy to demonstrate that under undrained and unrelaxed conditions,

$$B_1^\infty = \frac{a_{13}a_{23} - a_{33}a_{12}}{a_{22}a_{33} - a_{23}^2} \tag{119}$$

$$B_2^\infty = \frac{a_{12}a_{23} - a_{22}a_{13}}{a_{22}a_{33} - a_{23}^2}. \tag{120}$$

Since these B_i^∞ do not appear in the final result, we do not bother substituting in the a_{ij} constants from equations (90)–(95).

The continuity of fluid pressure $p_{f2} = p_{f1}$ along $\partial\Omega_{12}$ ($x = 0$) requires that $C_2 = B_1^\infty - B_2^\infty$. The definition of $\dot{\zeta}_{\rm int}$ may now be used to write

$$-i\omega\zeta_{\rm int} = \frac{1}{V}\int_{\partial\Omega_{12}} \frac{k_2}{\eta}\frac{\partial p_2}{\partial x} \tag{121}$$

$$= \frac{k_2}{\eta} i^{3/2}\sqrt{\frac{\omega}{D_2}}\frac{S}{V}(B_1^\infty - B_2^\infty)\Delta P \tag{122}$$

$$= i^{3/2}\sqrt{\omega}\sqrt{\frac{k_2\alpha_2}{\eta B_2 K_2^d}}\frac{S}{V}(\overline{p}_{f1} - \overline{p}_{f2}) \tag{123}$$

where we have used, to leading order in the high-frequency limit, that $\overline{p}_{f1} - \overline{p}_{f2} = (B_1^\infty - B_2^\infty)\Delta P$. The desired limit is thus $\lim_{\omega\to\infty}\gamma(\omega) = \sqrt{-i\omega k_2\alpha_2/(\eta B_2 K_s^d)}S/V$.

Full model for $\gamma(\omega)$

The high- and low-frequency limits are again causally connected via the simple function

$$\gamma(\omega) = \gamma_{sq}\sqrt{1 - \frac{i\omega}{\omega_{sq}}} \tag{124}$$

but now the parameters are defined as

$$\gamma_{sq} = \frac{v_2 k_2}{\eta L_2^2} \tag{125}$$

$$\omega_{sq} = \frac{B_2 K_2^d}{\eta\alpha_2}\frac{k_2}{L_2^2}\left(\frac{v_2 V/S}{L_2}\right)^2. \tag{126}$$

Squirt Flow Modeling Choices

To make numerical predictions of attenuation and dispersion, models must be proposed for the phase 2 (porous grain) parameters.

If the grains are modeled as spheres of radius R, the fluid-pressure gradient length within the grains can be estimated as $L_2 = R/\sqrt{15}$ and the volume to surface ratio as $V/S = R/(3v_2)$. The grain porosity is assumed to be in the form of microcracks and so it is natural to define an effective aperature h for these cracks. If the cracks have an average effective radius of R/N_R where N_R is roughly 2 or 3 and if there are on average N_c cracks per grain where N_c is also roughly 2 or 3 then the permeability and porsity of the grains is reasonably modeled as

$$\phi_2 = \frac{3N_c}{4N_R^2}\frac{h}{R} \quad \text{and} \quad k_2 = \phi_2 h^2/12 \tag{127}$$

where ϕ_2 is the fracture porosity within the porous grains. The dimensionless parameters k_2/L_2^2 and $(v_2 V/S)/L_2$ required in the expressions for γ_{sq} and ω_{sq} are given by

$$\frac{k_2}{L_2^2} = \frac{15N_c}{16N_R^2}\left(\frac{h}{R}\right)^3 \quad \text{and} \quad \left(\frac{v_2 V/S}{L_2}\right)^2 = \frac{5}{3}. \tag{128}$$

The normalized fracture aperature h/R is the key parameter in the squirt model.

The drained grain modulus K_2^d is necessarily a function of the crack porosity ϕ_2 (and therefore h/R). Real crack surfaces have micron (and smaller) scale asperities present upon them. If effective stress is applied in order to make the normalized aperature h/R smaller (so that, for example, the peak in squirt attenuation lies in the seismic band), new contacts are created that make the crack stronger. In the limit as $h/R \to 0$ (large effective stress), the cracks are no longer present and $K_2^d \to K_s$ where K_s is the mineral modulus of the grain.

Many models for such stiffening could be proposed. We intentionally make a conservative estimate here in proposing a simple linear porosity dependence $K_2^d = K_s(1-\sigma\phi_2)$, where σ is a fixed constant determined from fitting ultrasonic attenuation data. Effective medium theories [see, for example, Berryman *et al.* (2002)] predict that σ should be inversely proportional to the aspect ratios of the cracks present. As a crack closes and asperities are brought into contact, there is naturally a decrease in ϕ_2 but there should also be a decrease in σ due to the fact that the remaining crack porosity becomes more spherical as new asperities come into contact. Taking σ to be constant as crack porosity decreases is thus a minimalist estimate for how the drained modulus increases.

Thus, the porous-grain elastic properties are taken to be

$$K_2^d = K_s(1-\sigma\phi_2) \tag{129}$$

$$\alpha_2 = 1 - K_2^d/K_s \tag{130}$$

$$\frac{1}{B_2} = 1+\phi_2\frac{K_2^d}{K_f}\left(\frac{1-K_f/K_s}{1-K_2^d/K_s}\right) \tag{131}$$

where we have used the Gassmann fluid-substitution relations for α_2 and B_2. The overall drained modulus K of the collection of porous (cracked) grains can be modeled for example as

$$K = \frac{K_2^d(1-v_1)}{1+cv_1} \tag{132}$$

which is the same drained-modulus model as given in the appendix but with the solid grain modulus K_s replaced by the cracked grain modulus K_2^d.

Numerical Examples

In Fig. 4, we plot the P-wave attenuation predicted using the above model when the overall grain packing corresponds to a consolidated sandstone ($v_1 = 0.2$ and $c = 5$) having a permeability of 10 mD. For the grain properties we take $\sigma = 0.8/(5\times10^{-3})$, $3N_c/(4N_R^2) = 1$, and $K_s = 38$ GPa (quartz) as fixed constants. This σ value was chosen so that there would be an important peak in attenuation at ultrasonic frequencies and is taken to be the same for all values of h/R. The various curves can be thought of as being due to the application of effective stress. The peak in Q^{-1} near 1 MHz that is invariant to h/R is that due to the macroscopic Biot loss (fluid pressure equilibration at the scale of the wavelength). The peak that shifts with h/R is that due to the squirt flow.

This figure indicates that although the squirt mechanism is probably operative and perhaps even dominant at ultrasonic frequencies, it does not seem to be involved in explaining the observed levels of intrinsic attenuation in exploration work. For real cracks inside of real grains, the σ value will diminish with effective stress (i.e., with h/R), so that the effects of squirt in the seismic band are likely to be even less than shown in Fig. 4.

We next introduce the grain parameters k_2, ϕ_2, and K_2^d as modeled here along with the same overall drained modulus K into the model of Dvorkin *et al.* (1995) and compare the

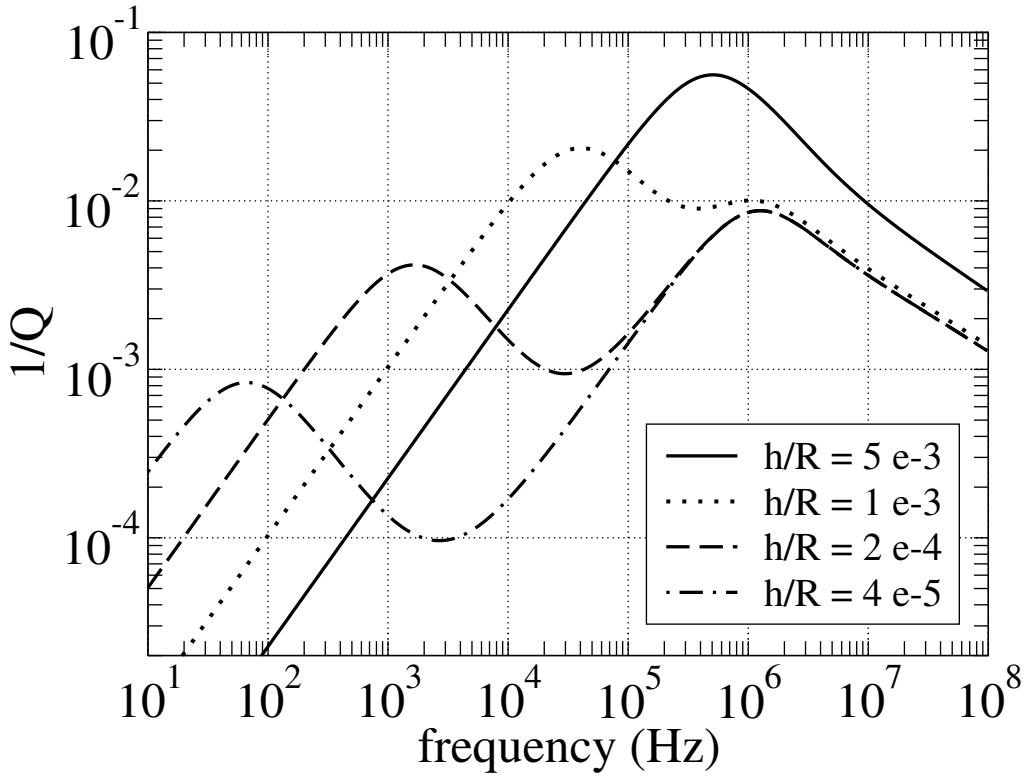

Figure 4: The squirt-flow model of P-wave attenuation when the grains are modeled as being spherical of radius R and containing microcracks having effective aperatures h. The overall drained modulus of the rock corresponds to a consolidated sandstone. jim3-nosquirt [NR]

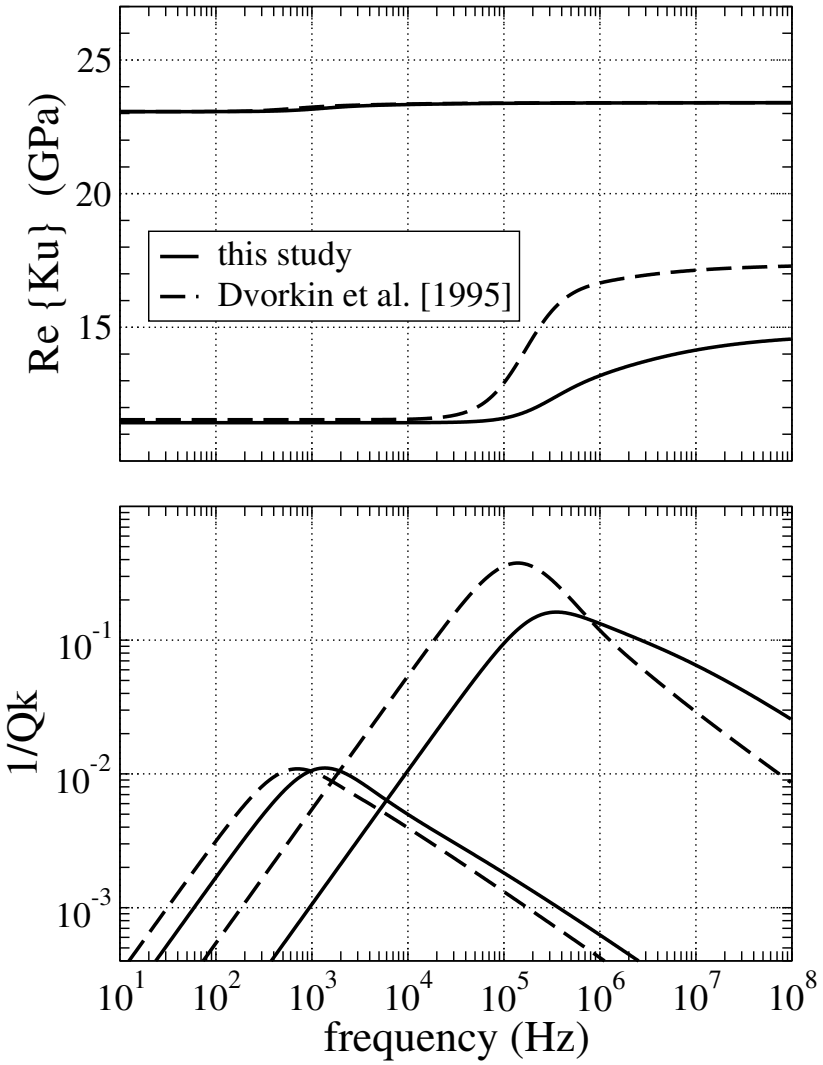

Figure 5: The undrained bulk modulus $K_U(\omega)$ in the squirt model of the present study and in the model of Dvorkin *et al.* (1995). The top graph is $\mathrm{Re}\{K_U\}$ while the bottom graph is $Q_K^{-1} = -2\mathrm{Im}\{K_U\}/\mathrm{Re}\{K_U\}$. The frame properties are the same as in Fig. 4. The curves having a smaller relaxation frequency ($\simeq 10^3$ Hz) and almost no dispersion correspond to $h/R = 2 \times 10^{-4}$ while the curves having the larger critical frequency ($\simeq 10^5$ Hz) and more dispersion correspond to $h/R = 5 \times 10^{-3}$. jim3-pridedvorkin [NR]

results to our own model for two different values of h/R (Fig. 5). Although both models have similar dependencies on the various material properties involved, there are nonetheless significant differences. These are principally due to the fact that the Dvorkin *et al.* (1995) model requires the grains to be in the form of effective cylinders of radius R, while in Fig. 5 we use a geometric parameter L_2 and volume-to-surface ratio V/S that are appropriate for spherically-shaped grains. However, in various limits as the frequency and/or fluid bulk modulus become either large or small, we have verified that both models yield qualitatively similar results.

CONCLUSIONS

Models for three different P-wave attenuation mechanisms were presented that differ only in the values of the a_{ij} constants and in the nature of the mesoscopic transport coefficient $\gamma(\omega)$. These three models correspond to (1) mesoscopic-scale heterogeneity in the frame moduli ("double porosity"), (2) mesoscopic-scale heterogeneity in the fluid type ("patchy-saturation"), and (3) grain-scale heterogeneity due to microcracks in the grains ("squirt"). In all three models, the amount of attenuation is controlled principally by the contrast of elastic compressibility among the constituents. In the double-porosity model, it is the contrast between the frame bulk-modulus of the two porous phases that is key, while in the patchy-saturation model it is the contrast in the fluid bulk modulus (immiscible patches of different fluids that have nearly identical bulk moduli would not produce much attenuation), and in the squirt model, it is the contrast between the drained modulus of an isolated cracked grain and that of the entire packing of grains.

Putting in small pockets of unconsolidated sand grains into an otherwise consolidated sandstone can produce attenuation in the seismic band that is comparable to what is measured in the field even when the pockets represent only a small amount of the total volume ($< 1\%$ volume fractions). Since mesoscopic-scale heterogeneity is rather ubiquitous throughout the earth's crust, it seems reasonable to suppose that this mechanism may be responsible for most of the attenuation observed in seismograms. The squirt mechanism produces a great deal of attenuation at the ultrasonic frequencies used in laboratory measurements, but has trouble explaining attenuation in the seismic band. This result is good news for some important applications of the theory because the mesoscopic-scale flow is affected by the permeability of the material, while squirt flow is not. This leaves open the possibility of extracting permeability information from the frequency dependence of seismically measured Q.

APPENDIX A. CONSTITUENT PROPERTIES

In order to use the unified double-porosity framework of the present paper, it is convenient to have models for the various porous-continuum constituent properties.

For unconsolidated sands and soils, the frame moduli (drained bulk modulus K^d and shear modulus G) are well modeled using the following variant of the Walton (1987) theory [*c.f.*,

Pride (2003) for details]

$$K^d = \frac{1}{6}\left[\frac{4(1-\phi_o)^2 n_o^2 P_o}{\pi^4 C_s^2}\right]^{1/3} \frac{(P_e/P_o)^{1/2}}{\left\{1+[16P_e/(9P_o)]^4\right\}^{1/24}}, \tag{133}$$

$$G = 3K^d/5, \tag{134}$$

where P_e is the effective overburden pressure [e.g., $P_e = (1-\phi)(\rho_s - \rho_f)gh$ where g is gravity and h is overburden thickness] and where P_o is the effective pressure at which all grain-to-grain contacts are established. For $P_e < P_o$, the coordination number n (average number of grain contacts per grain) is increasing as $(P_e/P_o)^{1/2}$. For $P_e > P_o$, the coordination number remains constant $n = n_o$. The parameter P_o is commonly on the order of 10 MPa. As $P_o \to 0$, the Walton (1987) result is obtained (all contacts in place starting from $P_e = 0$). The porosity of the grain pack is ϕ_o and the compliance parameter C_s is defined

$$C_s = \frac{1}{4\pi}\left(\frac{1}{G_s} + \frac{1}{K_s + G_s/3}\right) \tag{135}$$

where K_s and G_s are the mineral moduli of the grains. For unimodal grain-size distributions and random grain packs, one typically has $0.32 < \phi_o < 0.36$ and $8 < n_o < 11$.

For consolidated sandstones, the frame moduli are modelled in the present paper as [*c.f.*, Pride (2003) for details]

$$K^d = K_s \frac{1-\phi}{1+c\phi}, \tag{136}$$

$$G = G_s \frac{1-\phi}{1+3c\phi/2}. \tag{137}$$

The consolidation parameter c represents the degree of consolidation between the grains and lies in the approximate range $2 < c < 20$ for sandstones. If it is necessary to use a c greater than say 20 or 30, then it is probably better to use the modified-Walton theory.

The undrained moduli K^u and B are conveniently and exactly modeled using the Gassmann (1951) theory whenever the grains are isotropic and composed of a single mineral. The results are

$$B = \frac{1/K^d - 1/K_s}{1/K^d - 1/K_s + \phi(1/K_f - 1/K_s)}, \tag{138}$$

$$K^u = \frac{K^d}{1 - B(1 - K^d/K_s)}, \tag{139}$$

from which the Biot-Willis constant α may be determined to be $\alpha = 1 - K^d/K_s$. These Gassmann results are often called the "fluid-substitution" relations.

The dynamic permeability $k(\omega)$ as modeled by Johnson *et al.* (1987) is

$$\frac{k(\omega)}{k_o} = \left[\sqrt{1 - i\frac{4}{n_J}\frac{\omega}{\omega_c}} - i\frac{\omega}{\omega_c}\right]^{-1}, \tag{140}$$

where the relaxation frequency ω_c, which controls the frequency at which viscous-boundary layers first develop, is given by

$$\omega_c = \frac{\eta}{\rho_f F k_o}. \tag{141}$$

Here, F is exactly the electrical formation factor when grain-surface electrical conduction is not important and is conveniently (though crudely) modeled using Archie's law $F = \phi^{-m}$. The cementation exponent m is related to the distribution of grain shapes (or pore topology) in the sample and is generally close to 3/2 in clean sands, close to 2 in shaly sands, and close to 1 in rocks having fracture porosity. The parameter n_J is, for convenience, taken to be 8 (cylinder model of the porespace).

REFERENCES

Berryman, J. G., 1988, Seismic attenuation in fluid-saturated porous media: *PAGEOPH: Pure Appl. Geophys.* **128**, 423–432.

Berryman, J. G., and Milton, G. W., 1991, Exact results for generalized Gassmann's equations in composite porous media with two constituents: *Geophysics* **56**, 1950–1960.

Berryman, J. G., and Wang, H. F., 1995, The elastic coefficients of double-porosity models for fluid transport in jointed rock: *J. Geophys. Res.* **100**, 24611–24627.

Berryman, J. G., and Wang, H. F., 2000, Elastic wave propagation and attenuation in a double-porosity dual-permability medium: *Int. J. Rock Mech.* **37**, 63–78.

Berryman, J. G., Pride, S. R., and Wang, H. F., 2002, A differential scheme for elastic properties of rocks with dry or saturated cracks: *Geophys. J. Int.* **151**, 597–611.

Biot, M. A., 1956, Theory of propagation of elastic waves in a fluid-saturated porous solid. I. Low-frequency range: *J. Acoust. Soc. Am.* **28**, 168–178.

Biot, M. A., 1962, Mechanics of deformation and acoustic propgation in porous media: *J. Appl. Phys.* **33**, 1482–1498.

Biot, M. A., and Willis, D. G., 1957, The elastic coefficients of the theory of consolidation: *J. Appl. Mech.* **24**, 594–601.

Dvorkin, J., Mavko, G., and Nur, A., 1995, Squirt flow in fully saturated rocks: *Geophysics* **60**, 97–107.

Gassmann, F., 1951, Über die Elastizität poröser Medien: *Vierteljahrsschrift der Naturfoschenden Gesellschaft in Zürich* **96**, 1–23.

Gelinsky, S., and Shapiro, S. A., 1997, Dynamic-equivalent medium approach for thinly layered saturated sediments: *Geophys. J. Int.* **128**, F1–F4.

Gurevich, B., and Lopatnikov, S. L., 1995, Velocity and attenuation of elastic waves in finely latered porous rocks: *Geophys. J. Int.* **121**, 933–947.

Hashin, Z., and Shtrikman, S., 1961, Note on a variational approach to the theory of composite elastic materials: *J. Franklin Inst.* **271**, 336–341.

Hill, R., 1963, Elastic properties of reinforced solids: Some theoretical principles: *J. Mech. Phys. Solids* **11**, 357–372.

Johnson, D. L., 2001, Theory of frequency dependent acoustics in patchy-saturated porous media: *J. Acoust. Soc. Am.* **110**, 682–694.

Johnson, D. L., Koplik, J., and Dashen, R., 1987, Theory of dynamic permability and tortuosity in fluid-saturated porous media: *J. Fluid Mech.* **176**, 379–402.

Mavko, G., and Nur, A., 1979, Wave attenuation in partially saturated rocks: *Geophysics* **44**, 161–178.

Norris, A. N., 1993, Low frequency dispersion and attenuation in partially saturated rocks: *J. Acoust. Soc. Am.* **94**, 359–370.

Pride, S. R., 2003, Relationships between seismic and hydrological properties: in *Hydrogeophysics*, edited by Y. Rubin and S. Hubbard, pp. 1–31, Kluwer, New York.

Pride, S. R., and Berryman, J. G., 2003a, Linear dynamics of double-porosity dual-permeability materials. I. Governing equations and acoustic attenuation: *Phys. Rev. E* **68**, 036603 (September 9, 2003).

Pride, S. R., and Berryman, J. G., 2003b, Linear dynamics of double-porosity dual-permeability materials. II. Fluid transport equations: *Phys. Rev. E* **68**, 036604 (September 9, 2003).

Pride, S. R., and Flekkoy, E. G., 1999, Two-phase flow through porous media in the fixed-contact line regime: *Phys. Rev. E* **60**, 4285–4299.

Quan, Y., and Harris, J. M, 1997, Seismic attenuation tomography using the frequency shift method: *Geophysics* **62**, 895–905.

Sams, M. S., Neep, J. P, Worthington, M. H., and King, M. S., 1997, The measurement of velocity dispersion and frequency-dependent intrinsic attenuation in sedimentary rocks: *Geophysics* **62**, 1456–1464.

Walton, K., 1987, The effective elastic moduli of a random packing of spheres: *J. Mech. Phys. Solids* **35**, 213–226.

White, J. E., Mikhaylova, N. G., and Lyakhovitsky, F. M., 1975, Low-frequency seismic waves in fluid-saturated layered rocks: *Izvestija Academy of Sciences USSR, Phys. Solid Earth* **11**, 654–659.

Williams, K. L., Jackson, D. R., Thorsos, E. I., Tang, D., and Schock, S. G., 2002, Comparison of sound speed and attenuation measured in a sandy sediment to predictions based on the Biot theory of porous media: *IEEE J. Ocean. Eng.* **27**, 413–428.